PROCEEDINGS OF SCIENCE

Non-perturbative thermal QCD at very high temperatures

Leonardo Giusti,[a,b,*] **Matteo Bresciani,**[a,b] **Mattia Dalla Brida,**[a,b] **Tim Harris,**[d] **Davide Laudicina,**[c] **Michele Pepe**[b] **and Pietro Rescigno**[a,b]

[a] *Dipartimento di Fisica, Università di Milano-Bicocca, Piazza della Scienza 3, I-20126 Milano, Italy*
[b] *INFN, Sezione di Milano-Bicocca, Piazza della Scienza 3, I-20126 Milano, Italy*
[c] *Fakultät für Physik und Astronomie, Institut für Theoretische Physik II, Ruhr-Universität Bochum, 44780 Bochum, Germany*
[d] *Institute for Theoretical Physics, ETH Zürich, Wolfgang-Pauli-Str. 27, 8093 Zürich, Switzerland*
E-mail: leonardo.giusti@unimib.it, davide.laudicina@ruhr-uni-bochum.de, m.bresciani9@campus.unimib.it, mattia.dallabrida@unimib.it, harrist@phys.ethz.ch, michele.pepe@mib.infn.it, p.rescigno1@campus.unimib.it

We present a recently introduced strategy to study non-perturbatively thermal QCD up to temperatures of the order of the electro-weak scale, combining step scaling techniques and shifted boundary conditions. The former allow to renormalize the theory for a range of scales which spans several orders of magnitude with a moderate computational cost. Shifted boundary conditions avoid the need for the zero temperature subtraction in the Equation of State. As a consequence, the simulated lattices do not have to accommodate two very different scales, the pion mass and the temperature. Effective field theory arguments guarantee that finite volume effects can be kept under control safely. As a first application of this strategy, we present the results of the computation of the hadronic screening spectrum in QCD with $N_f = 3$ flavours of massless quarks for temperatures from $T \sim 1$ GeV up to ~ 160 GeV.

42nd International Conference on High Energy Physics (ICHEP2024)
18-24 July 2024
Prague, Czech Republic

*Speaker

PoS(ICHEP2024)503

1. Introduction

Quantum Chromodynamics (QCD) at very high temperatures plays a pivotal rôle in particle and nuclear physics as well as in cosmology. In order to have a reliable and satisfactory understanding of the dynamics of the high temperature regime of QCD, a fully non-perturbative approach is essential up to temperatures as high as the electro-weak scale [1–3]. Here we present a strategy, first introduced for the Yang-Mills theory in Ref. [2] and then generalized to QCD in Ref. [3], which allows to simulate the theory of strong interactions up to very high temperatures from first principles with a moderate computational effort. As a first concrete implementation in QCD, we report the results that we have obtained for the hadronic screening masses with $N_f = 3$ massless quarks in a temperature interval ranging from $T \sim 1$ GeV up to ~ 160 GeV [3, 4]. Those observables probe the exponential fall-off of two-point correlation functions of hadronic interpolating operators in the spatial directions and are the inverses of spatial correlation lengths, which characterize the response of the plasma when hadrons are injected into it.

2. Non-perturbative thermal QCD at very high temperatures

Renormalization and lines of constant physics – A hadronic scheme is not a convenient choice to renormalize QCD non-perturbatively when considering a broad range of temperatures spanning several orders of magnitude. This would require to accommodate on a single lattice both the temperature and the hadronic scale which may differ by orders of magnitude, making the numerical computation extremely challenging. A similar problem is encountered when renormalizing QCD non-perturbatively, and it was solved many years ago by introducing a step-scaling technique [5].

In order to solve our problem, we have built on that knowledge by considering a non-perturbative definition of the coupling constant, $\bar{g}^2_{\rm SF}(\mu)$, which can be computed precisely on the lattice for values of the renormalization scale μ which span several orders of magnitude. Making a definite choice, in this section we use the definition based on the Schrödinger functional (SF) [5], however, notice that other theoretically equivalent choices are available. In particular, in our lattice setup we also made use of the gradient flow (GF) definition of the running coupling [6, 7], see appendix B of Ref. [3]. Once $\bar{g}^2_{\rm SF}(\mu)$ is known in the continuum limit for $\mu \sim T$ [6, 8], thermal QCD can be renormalized by fixing the value of the running coupling constant at fixed lattice spacing a, $g^2_{\rm SF}(g_0^2, a\mu)$, to be

$$g^2_{\rm SF}(g_0^2, a\mu) = \bar{g}^2_{\rm SF}(\mu) \ , \qquad a\mu \ll 1 \ . \tag{1}$$

This condition fixes the so-called lines of constant physics, i.e. the dependence of the bare coupling constant g_0^2 on the lattice spacing, for values of a at which the scale μ and therefore the temperature T can be easily accommodated. For a more complete discussion on how this technique is implemented in practical lattice simulations we refer to appendix B of Ref. [3].

Shifted boundary conditions – The thermal theory is defined by requiring that the fields satisfy shifted boundary conditions in the compact direction [9–11], while we set periodic boundary conditions in the spatial directions. The former consist in shifting the fields by the spatial vector $L_0\,\boldsymbol{\xi}$ when crossing the boundary in the compact direction, with the fermions having in addition the usual sign flip. For the gauge fields they read

$$U_\mu(x_0 + L_0, \boldsymbol{x}) = U_\mu(x_0, \boldsymbol{x} - L_0\boldsymbol{\xi}) \ , \quad U_\mu(x_0, \boldsymbol{x} + \hat{k} L_k) = U_\mu(x_0, \boldsymbol{x}) \ , \tag{2}$$

while those for the quark and the anti-quark fields are given by

$$\begin{aligned} \psi(x_0 + L_0, \boldsymbol{x}) &= -\psi(x_0, \boldsymbol{x} - L_0\boldsymbol{\xi}) \ , & \psi(x_0, \boldsymbol{x} + \hat{k}L_k) &= \psi(x_0, \boldsymbol{x}) \ , \\ \bar{\psi}(x_0 + L_0, \boldsymbol{x}) &= -\bar{\psi}(x_0, \boldsymbol{x} - L_0\boldsymbol{\xi}) \ , & \bar{\psi}(x_0, \boldsymbol{x} + \hat{k}L_k) &= \bar{\psi}(x_0, \boldsymbol{x}) \ , \end{aligned} \tag{3}$$

where L_0 and L_k are the lattice extent in the 0 and k-directions respectively. In the thermodynamic limit, a relativistic thermal field theory in the presence of a shift $\boldsymbol{\xi}$ is equivalent to the very same theory with usual periodic (anti-periodic for fermions) boundary conditions but with a longer extension of the compact direction by a factor $\sqrt{1+\boldsymbol{\xi}^2}$ [11], and thus the standard relation between the length and the temperature is modified as $T = 1/(L_0\sqrt{1+\boldsymbol{\xi}^2})$. Shifted boundary conditions represent a very efficient setup to tackle several problems that are otherwise very challenging both from the theoretical and the numerical viewpoint. Some recent examples are provided by the SU(3) Yang-Mills theory Equation of State (EoS) which was obtained with a permille precision up to very high temperatures [2, 12] and more recently in $N_f = 3$ QCD with a novel computation of the renormalization constant of the flavour-singlet local vector current [13]. The same setup is currently in use to carry out the first non-perturbative computation of the EoS at large temperatures in thermal QCD [14, 15].

Finite-volume effects – At asymptotically high temperatures, the mass gap developed by thermal QCD is proportional to g^2T. On the other hand, at intermediate temperatures, provided that the temperature is sufficiently large with respect to $\Lambda_{\rm QCD}$, the mass gap of the theory is always expected to be proportional to the temperature times an appropriate power of the coupling constant. As a consequence, when $LT \to \infty$ finite-size effects are exponentially suppressed in LT times a coefficient that decreases logarithmically with the temperature. For this reason, we have always employed large spatial extents, i.e. $L/a = 288$, so that LT ranges always from 20 to 50.

Restricting to the zero-topological sector – At high temperature, the topological charge distribution is expected to be highly peaked at zero. For QCD with three light degenerate flavours of mass m, the dilute instanton gas approximation predicts for the the topological susceptibility $\chi \propto m^3T^{-b}$ with $b \sim 8$. The analogous prediction for the Yang–Mills theory has been verified explicitly on the lattice [16]. Similarly, computations performed in QCD seem to confirm the T-dependence predicted by the semi-classical analysis even though the systematics due to the introduction of dynamical fermions is still difficult to control [17]. As a result, already at low temperatures, namely at $T \sim 1$ GeV, the probability to encounter a configuration with non-zero topology in volumes large enough to keep finite volume effects under control is expected to be several orders of magnitude smaller than the permille or so. For these reasons, we can safely restrict our calculations to the sector with zero topology.

3. Screening spectrum

As a concrete application of the strategy outlined in section 2, we have performed numerical simulations at 12 values of the temperature, $T_0, \ldots, T_{11}$ covering the range from approximately 1 GeV up to about 160 GeV. For the 9 highest ones, $T_0, \ldots, T_8$, gluons are regularized with the Wilson plaquette action, while for the 3 lowest temperatures, T_9, T_{10} and T_{11}, we adopt the tree-level improved Lüscher-Weisz gauge action. The three massless flavours are always discretized by the $O(a)$-improved Wilson–Dirac operator. In order to extrapolate the results to the continuum limit,

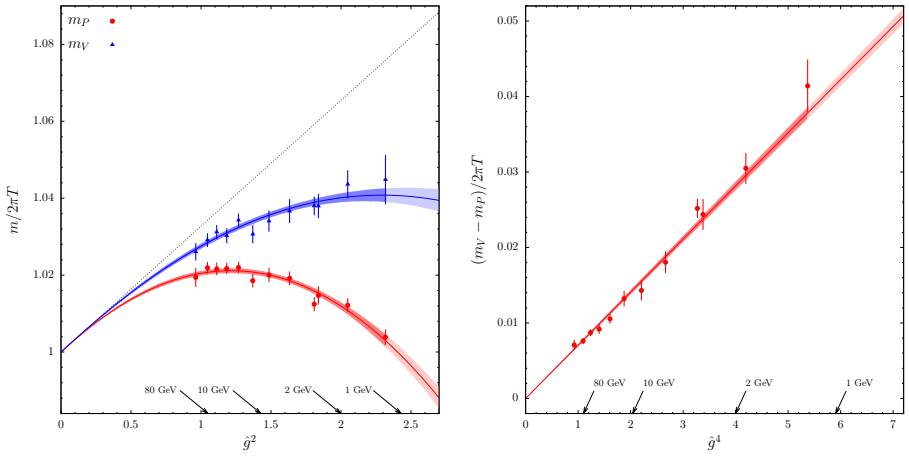

Figure 1: Left: pseudoscalar (red) and vector (blue) screening masses versus $\hat{g}^2$. The bands represent the best fits in Eqs. (5) and (7), while the dashed line is the analytically known contribution. Right: the vector-pseudoscalar mass difference, normalized to $2\pi T$, versus $\hat{g}^4$. Red bands represent the best fits of the data as explained in the text.

several lattice spacings are simulated at each temperature with the extension of the fourth dimension being $L_0/a = 4, 6, 8$ or 10.

Mesonic screening masses – The mesonic screening masses have been computed with a few permille accuracy in the continuum limit. Within our statistical precision, the screening masses associated to the pseudoscalar and to the scalar density are found to be degenerate and a similar discussion holds for the screening masses of the vector and of the axial current as expected in the presence of chiral symmetry restoration. Given the high accuracy of our non-perturbative data, it has been possible to parameterize the temperature dependence of the masses. In order to do that, we have introduced the function $\hat{g}^2(T)$ defined as

$$\frac{1}{\hat{g}^2(T)} \equiv \frac{9}{8\pi^2}\ln\frac{2\pi T}{\Lambda_{\overline{\rm MS}}} + \frac{4}{9\pi^2}\ln\left(2\ln\frac{2\pi T}{\Lambda_{\overline{\rm MS}}}\right)\,, \tag{4}$$

where $\Lambda_{\overline{\rm MS}} = 341$ MeV is taken from Ref. [18]. It corresponds to the 2-loop definition of the strong coupling constant in the $\overline{\rm MS}$ scheme at the renormalization scale $\mu = 2\pi T$. For our purposes, however, this is just a function of the temperature T that we use to analyze our results and which makes it easier to compare with the known perturbative results.

The temperature dependence of the pseudoscalar mass has been parameterized with a quartic polynomial in $\hat{g}$ of the form

$$\frac{m_P}{2\pi T} = p_0 + p_2\hat{g}^2 + p_3\hat{g}^3 + p_4\hat{g}^4\,. \tag{5}$$

The leading and the quadratic coefficients have been found to be compatible with the free theory value and the next-to-leading order correction, i.e. $p_0 = 1$ and $p_2 = 0.0327$ [19]. Once p_0 and p_2 have been fixed to their corresponding perturbative values, we obtain for the cubic and the quartic fit parameters $p_3 = 0.0038(22)$ and $p_4 = -0.0161(17)$ with $\mathrm{cov}(p_3, p_4)/[\sigma(p_3)\sigma(p_4)] = -1.0$ with an excellent $\chi^2/\mathrm{dof} = 0.75$. Such a polynomial is displayed, as a red band, together with the non-perturbative data in the left panel of Figure 1. It is clear that the quartic term is necessary to

explain the behaviour of the non-perturbative data in the entire temperature range. In particular, at the highest temperatures it contributes for about 50% of the total contribution due to the interactions, while at low temperature it competes with the quadratic coefficient to bend down $m_P/2\pi T$.

The mass difference between the vector and the pseudoscalar mass is due to spin-dependent contributions which are of $O(g^4)$ in the effective field theory. By plotting our results versus $\hat{g}^4$, see right panel of Figure 1, these turn out to lie on a straight line with vanishing intercept in the entire range of temperature. We then parameterized the temperature dependence with

$$\frac{(m_V - m_P)}{2\pi T} = s_4\,\hat{g}^4 \tag{6}$$

and we obtain $s_4 = 0.00704(14)$ with $\chi^2/\mathrm{dof} = 0.79$. It is remarkable that, even at the highest temperatures which was simulated, the mass difference is clearly different from zero, a fact which is not expected by the next-to-leading order estimate obtained in the effective field theory. The best parameterization for the vector screening mass is thus given by

$$\frac{m_V}{2\pi T} = p_0 + p_2\,\hat{g}^2 + p_3\,\hat{g}^3 + (p_4 + s_4)\,\hat{g}^4\,, \tag{7}$$

with covariances $\mathrm{cov}(p_3, s_4)/[\sigma(p_3)\sigma(p_4)] = 0.08$ and $\mathrm{cov}(p_4, s_4)/[\sigma(p_4)\sigma(p_4)] = -0.07$. In the vector channel the quartic contribution appearing in Eq. (7) is responsible for about 15% of the total contribution due to interaction at the electro-weak scale. Moreover, the quartic coefficient for the vector mass is about 50% smaller than the corresponding coefficient for the pseudoscalar channel. As a consequence, its contribution is not large enough to compete with the quadratic coefficient and to bend down the value of the vector mass at low temperature. For a detailed analysis of the results see section 7 of Ref. [3].

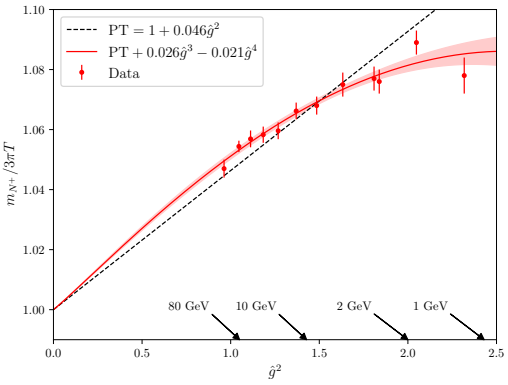

Figure 2: Nucleon screening mass versus $\hat{g}^2$. The band represent the best fit to Eq. (8), while the dashed line is the analytically known contribution.

Baryonic screening masses – In contrast with the mesonic case, there are very few studies on the baryonic sector both on the lattice and in the three dimensional effective theory and, for what concerns lattice calculations, no continuum limit extrapolation has ever been performed. In Ref. [4] we have computed the baryonic screening masses for the first time in the continuum limit and with a final accuracy of a few permille from 1 GeV up to the electro-weak scale. As expected in a chirally symmetric regime, the positive and the negative parity screening masses are found to be degenerate in the entire range of temperatures. For this reason, in the following we only focus on the positive parity mass m_{N^+}. The final results are shown in Figure 2 as a function of $\hat{g}^2(T)$.

As it is clear from the plot, the bulk of the baryonic screening mass is given by the free field theory $3\pi T$ plus a $4-8\%$ positive contribution due to interaction. It is rather clear that from $T \sim 160$ GeV down to $T \sim 5$ GeV the perturbative expression is within half a percent with respect to the non-perturbative data. The full set of data, however, shows a distinct negative curvature which

requires higher orders in the coupling constant to be parameterized. Similarly to the case of the mesonic screening masses, the temperature dependence of the baryonic screening mass has been parameterized with the ansatz

$$\frac{m_{N^+}}{3\pi T} = b_0 + b_2\,\hat{g}^2 + b_3\,\hat{g}^3 + b_4\,\hat{g}^4\ . \tag{8}$$

The coefficients b_0 and b_2 turn out to be compatible with the free-theory and the next-to-leading values, i.e. $b_0 = 1$ and $b_2 = 0.046$ [20]. Then, by enforcing those values and fitting again, we obtain $b_3 = 0.026(4)$, $b_4 = -0.021(3)$ and $\mathrm{cov}(b_3, b_4)/[\sigma(b_3)\sigma(b_4)] = -0.99$ with $\chi^2/\mathrm{dof} = 0.64$, which is the best parameterization of our results over the entire range of temperatures explored. Notice that, in general, other parameterizations of the lattice data are possible as well. These, however, result in the disagreement between the fit result for b_2 and the 1-loop perturbative correction. For a more detailed discussion on such parameterizations we refer to section 5 of Ref. [4].

We conclude by noticing that the evaluation of the EoS in a similar temperature range, computed with the strategy outlined in Ref. [15], is almost completed. Preliminary results shown at the conference are not reported here for lack of space.

References

[1] K. Kajantie, M. Laine, K. Rummukainen, and Y. Schröder, *Phys. Rev. D* **67** (2003) 105008.

[2] L. Giusti and M. Pepe, *Phys. Lett.* **B769** (2017) 385.

[3] M. Dalla Brida, L. Giusti, T. Harris, D. Laudicina, and M. Pepe, *JHEP* **04** (2022) 034.

[4] L. Giusti et al., *Phys. Lett. B* **855** (2024) 138799.

[5] M. Lüscher, R. Sommer, P. Weisz, and U. Wolff, *Nucl. Phys.* **B413** (1994) 481.

[6] **ALPHA** Collaboration, M. Dalla Brida et al., *Phys. Rev. Lett.* **117** (2016) no. 18 182001.

[7] **ALPHA** Collaboration, M. Dalla Brida et al., *Phys. Rev. D* **95** (2017) no. 1 014507.

[8] **ALPHA** Collaboration, M. Dalla Brida et al., *Eur. Phys. J. C* **78** (2018) no. 5 372.

[9] L. Giusti and H. B. Meyer, *JHEP* **11** (2011) 087.

[10] L. Giusti and H. B. Meyer, *Phys. Rev. Lett.* **106** (2011) 131601.

[11] L. Giusti and H. B. Meyer, *JHEP* **01** (2013) 140.

[12] L. Giusti and M. Pepe, *Phys. Rev. Lett.* **113** (2014) 031601.

[13] M. Bresciani et al., *Phys. Lett. B* **835** (2022) 137579.

[14] M. Dalla Brida, L. Giusti, and M. Pepe, *JHEP* **04** (2020) 043.

[15] M. Bresciani et al., in *41st International Symposium on Lattice Field Theory*, 2024.

[16] L. Giusti and M. Lüscher, *Eur. Phys. J. C* **79** (2019), no. 3 207.

[17] S. Borsanyi et al., *Nature* **539** (2016), no. 7627 69.

[18] **ALPHA** Collaboration, M. Bruno et al., *Phys. Rev. Lett.* **119** (2017), no. 10 102001.

[19] M. Laine and M. Vepsalainen, *JHEP* **02** (2004) 004.

[20] L. Giusti et al., *JHEP* **06** (2024) 205.